Chinese Chemical Letters 36 (2025) 110380

Contents lists available at ScienceDirect

Chinese Chemical Letters

journal homepage: www.elsevier.com/locate/cclet

Degradation of chloroxylenol by CoS_x activated peroxomonosulfate: Role of cobalt-sulfur ratio

Jiayi Guo[a], Liangxiong Ling[a], Qinwei Lu[a], Yi Zhou[a], Xubiao Luo[b], Yanbo Zhou[a,b,c,*]

[a] State Environmental Protection Key Laboratory of Environmental Risk Assessment and Control on Chemical Process, East China University of Science and Technology, Shanghai 200237, China
[b] School of Life Sciences, Key Laboratory of Jiangxi Province for Functional Biology and Pollution Control in Red Soil Regions, Jinggangshan University, Ji'an 343009, China
[c] State Key Laboratory of Coal Liquification, Gasification and Utilization with High Efficiency and Low Carbon Technology, Shanghai 200237, China

ARTICLE INFO

Article history:
Received 22 May 2024
Revised 23 July 2024
Accepted 28 August 2024
Available online 29 August 2024

Keywords:
Peroxymonosulfate
Fenton-like reaction
Cobalt sulfides
Chloroxylenol degradation
Morphology control

ABSTRACT

Cobalt sulfide has received widespread attention in the advanced oxidation treatment of wastewater, and its catalytic activity is influenced by crystal structure and exposed active sites. This work successfully constructed three types of cobalt sulfides, namely Co_9S_8, Co_3S_4 and CoS_2, by changing the molar ratio of cobalt to sulfur. The results showed that the degradation efficiency of Co_9S_8, Co_3S_4 and CoS_2 on chloroxylenol by activated peroxomonosulfate (PMS) were 100%, 88.70% and 67.73%, respectively. Combined with density functional theory (DFT), the structural properties and reaction energy barriers of different cobalt-sulfur ratios were calculated. As the ratio of cobalt to sulfur increases, the sulfur vacancies realized a fuller exposure of active sites ($Co^{2+}_{surf.}$) on the surface of the catalysts, with a highly linear relationship with the reaction rate constant ($R^2 = 0.945$). This work explores the structure-activity relationship between cobalt sulfur ratio and degradation efficiency, which can guide new catalyst synthesis.

In recent years, there is a continuous growth of the demand for personal care products with antibacterial effects. Thus, various germicidal ingredients are widely added to hand sanitizers, soaps, and body lotions [1,2]. As a typical alternative to traditional bactericides (such as triclosan and triclocarban), the antiviral efficacy of chloroxylenol (PCMX) against the novel coronavirus (COVID-19) has been demonstrated, which was significant used in recent years [3,4]. Notably, PCMX has stable chemical properties, and could reach a certain cumulative concentration in the environment. PCMX (at concentrations of 1.46–5.59 μg/L) has been reported to be detected in influent water from wastewater treatment plants [5,6]. Despite the low concentrations detected, PCMX can cause significant harm to the aquatic environment and human health due to its biological activity [7].

Advanced oxidation processes (AOPs) that generate strong oxidizing free radicals (*e.g.*, $SO_4^{\bullet-}$ and $^{\bullet}OH$) have received much attention in degrading of organic pollutants in water [8-10]. Transition metals (Co, Fe, Mn, Cu, *etc.*) are widely used as catalysts for oxidative degradation due to their variable valence states, which active oxidizing agent mainly by single electron transfer [11,12]. Cobalt-based catalysts are considered to be the most effective catalysts among various transition metal [13,14]. Reduced sulfur species can accelerate the M(II)/M(III) cycle, thereby further improving the production and conversion efficiency of related reactive oxygen species (ROS) and improving catalytic performance [15,16].

The efficient degradation of organic pollutants in wastewater by cobalt sulfide-activated peroxymonosulfate (PMS) has attracted much attention [17,18]. Previous studies have shown that different crystal types of CoS_x affect the catalytic degradation performance, and the design and modulation of cobalt-based catalysts with abundant active sites is an effective strategy to obtain efficient cobalt-based catalysts [19,20]. However, there are few reports investigating the effects of different cobalt-sulfur molar ratios on cobalt sulfide catalysts with tunable morphology and crystal structure, while the relationship between the physical properties of different CoS_x and their catalytic reaction efficiencies is still poorly understood. Therefore, the aim of this work is to investigate the effect of precursor molar ratio on the physical properties of CoS_x and the structure-performance conformational relationship for PMS activation.

In this work, CoS_x with three different cobalt-sulfur molar ratios were fabricated and characterized by a one pot method. The degradation performance of PCMX by CoS_x activated PMS was systematically evaluated, including process parameters and reaction

* Corresponding author.
E-mail addresses: zhouyanbo@ecust.edu.cn, yanbo_zhou@163.com (Y. Zhou).

https://doi.org/10.1016/j.cclet.2024.110380
1001-8417/

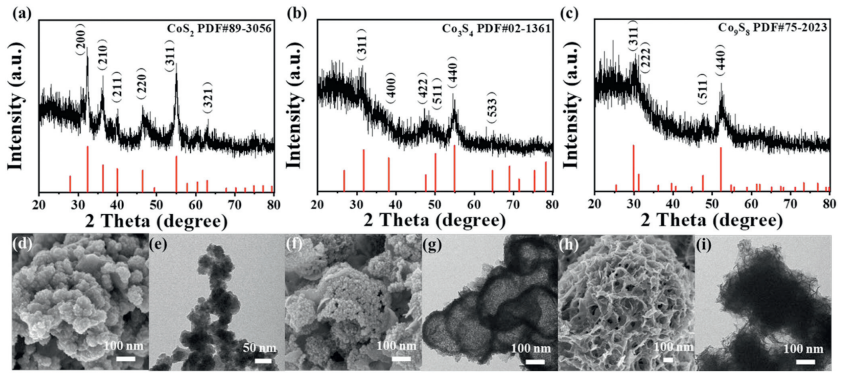

Fig. 1. XRD patterns, FESEM images, and TEM images of (a, d, e) CoS_2, (b, f, g) Co_3S_4, and (c, h, i) Co_9S_8.

mechanism combined with density functional theory (DFT), the effect of cobalt sulfide ratio on catalyst reactivity were systematically studied.

All detailed chemicals, experimental and characterization methods are provided in Text S1 (Supporting information).

Three kinds of cobalt sulfide were simply synthesized by changing the ratio of cobalt to sulfur in the synthesis process. The crystal structure of CoS_x was characterized by X-ray diffractometer (XRD). The XRD patterns were well matched with CoS_2 (PDF #89-3056), Co_3S_4 (PDF #02-1361), and Co_9S_8 (PDF #75-2023), respectively. It indicates that CoS_x with different crystal structures were successfully synthesized by facile varying cobalt-sulfur ratio (Figs. 1a–c). The crystal structure of CoS_2, Co_3S_4, and Co_9S_8 is shown in Fig. S1 (Supporting information).

The scanning electron microscope (SEM) and transmission electron microscope (TEM) images show that CoS_2 appears as nanospheres (Figs. 1d and e), Co_3S_4 appears as hollow nanospheres (Figs. 1f and g), and Co_9S_8 exhibits nanoflowers morphology (Figs. 1h and i). The results show that the controllable preparation of CoS_x morphology can be achieved by adjusting cobalt-sulfur ratio. Inductive coupled plasma-optical emission spectrometry (ICP-OES) (Table S1 in Supporting information) turns out that the true cobalt-sulfur molar ratios of CoS_2, Co_3S_4, and Co_9S_8 are 1:2.0, 1:1.5, and 1:1.1, respectively. The Brunauer-Emmett-Teller (BET) surface area and pore structure of catalysts were analyzed using N_2 adsorption-desorption isotherms and BJH pore size distribution (Fig. S2 in Supporting information), which indicates the mesoporous structures of both three catalysts. The above results conform to their theoretical ratios and provide further evidence for the successful preparation of CoS_x nanocatalyst as well. BET surface area, pore volume, and pore size of the three catalysts are shown in Table S2 (Supporting information). Obviously, the controllable preparation of CoS_x morphology and the corresponding crystal structure can be realized by adjusting the ratio of cobalt(II) acetate tetrahydrate and thiourea.

Fig. 2a shows the effects of different catalysts CoS_x on PCMX degradation *via* PMS activation. The adsorption ability of the pure CoS_2, Co_3S_4, or Co_9S_8 on PMCX was negligible (3.1%, 3.9%, and 1.3%, respectively). This finding is consistent with those of Lu *et al.* and Li *et al.* who found that pure PMS and pure CoS_x had a weak adsorption capacity for pollutants [21,22]. The degradation efficiencies of CoS_2, Co_3S_4, or Co_9S_8 on PCMX by PMS activation were 67.7%, 88.7% and 100%, respectively, which indicated that Co_9S_8 exposed more PMS activation sites than Co_3S_4 and CoS_2 under the same catalyst dosage conditions. It has been reported that $Co^{2+}_{surf.}$ exposed on the surface of cobalt-based catalysts could participate in the activation of PMS, which significantly enhanced the degradation efficiency [23].

The kinetic simulation results showed that the degradation behavior of PCMX was better fitted with the *pseudo*-first-order kinetic model (Table S3 in Supporting information). The degradation rate of PCMX was obviously accelerated with the increase of cobalt-sulfur ratio (Fig. 2b). The reaction rate constants of PCMX degradation in CoS_2/PMS, Co_3S_4/PMS, and Co_9S_8/PMS were 0.0386 min^{-1}, 0.1619 min^{-1} and 2.3026 min^{-1}, respectively. The decomposition efficiency of PMS by CoS_x with time was in agreement with that of PCMX degradation in CoS_x/PMS systems, as shown in Fig. 2c. CoS_2 had a relatively weak activation ability for PMS, with a decomposition efficiency of 57.6% at 30 min, while Co_3S_4 and Co_9S_8 were able to decompose PMS almost completely at 30 min and 5 min, respectively. It may be attributed to the lower sulfation degree of Co_9S_8, which facilitates the exposure of its surface active sites ($Co^{2+}_{surf.}$) to promote the decomposition of PMS.

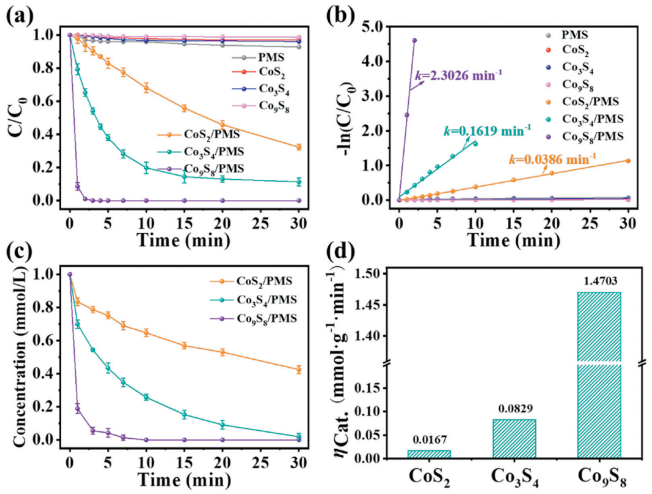

Fig. 2. (a) PCMX removal curves in different systems. (b) The *pseudo*-first-order kinetic rate plots of PCMX degradation in CoS_2/PMS, Co_3S_4/PMS, and Co_9S_8/PMS systems. (c) PMS residual concentration in each system. (d) Utilization efficiency of different cobalt sulfides. Conditions: $[Cat.]_0 = 0.20$ g/L, $[PCMX]_0 = 20$ mg/L, $[PMS]_0 = 1.00$ mmol/L, $pH_0 = 6.6$, $T = 20 \pm 1$ °C).

To further determine the catalytic activity of the materials, the catalyst utilization efficiency ($\eta_{Cat.}$), the molar mass of pollutant degraded per gram of catalyst per minute, was calculated (Eq. 1). The calculation results are shown in Fig. 2d. The CoS_x nanocatalysts prepared in this study showed high degradation activity for PCMX compared to previously reported cobalt-based catalysts (Table S4 in Supporting information). Among the CoS_x, Co_9S_8 could completely remove PCMX within 3 min, and its $\eta_{Cat.}$ reached 1.4703 mmol g^{-1} min^{-1}.

$$\eta_{Cat.}\left(\frac{mmol}{g \cdot min}\right) = \frac{\Delta[pollutant]}{[Cat.]} \times k \quad (1)$$

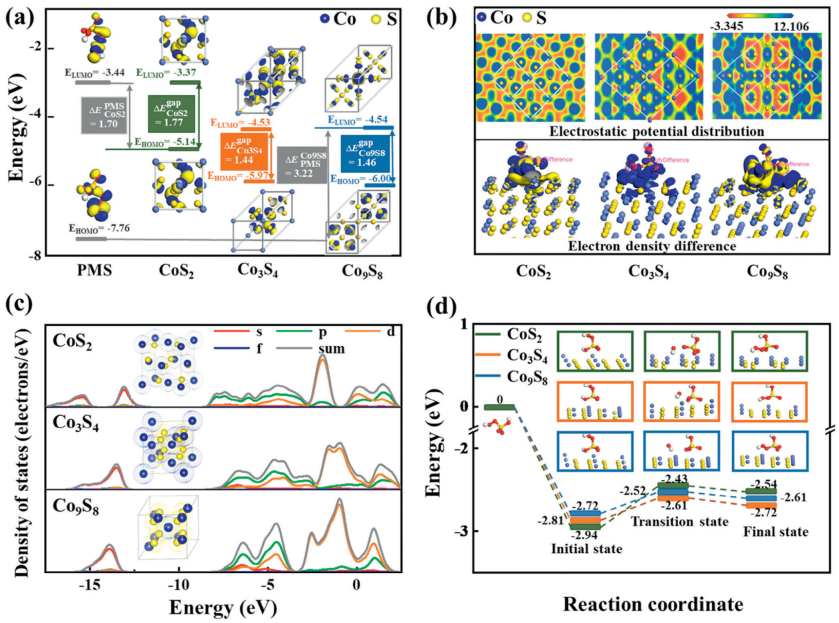

Fig. 3. (a) LUMO, HOMO and LUMO-HOMO gap energy levels of CoS_x and PMS. (b) Electrostatic potential distribution of CoS_x; Electron density differences of different PMS adsorption models. Isosurface contour is 0.005 e/bohr^3. (c) Density of states of CoS_x. (d) The corresponding reaction energy barriers for PMS activation.

In order to further explore the reactivity of catalysts with different crystal forms caused by cobalt-sulfur ratio, DFT calculations were performed on reaction energy levels and electronic properties [24]. By calculating $\Delta E_{Cat.}^{PMS}$ (energy level gap between catalyst and PMS), it can be seen that the energy level difference between CoS_2 and PMS is narrower ($\Delta E_{CoS_2}^{PMS} = 1.70$ eV), which proves that PMS can more easily receive electrons transferred from CoS_2 (Fig. 3a) [25-27]. This $\Delta E_{Co_9S_8}^{gap}$ (HOMO-LUMO gap) is similar to $\Delta E_{Co_3S_4}^{gap}$, and is significantly lower than CoS_2, indicating that the increase of cobalt to sulfur ratio makes the catalyst's reactivity significantly enhanced.

Electrostatic potential distribution (E_{SP}) shows that there are great differences in the charge distribution on the surface of the catalyst with different cobalt-sulfur ratios (Fig. 3b). The results show that this cobalt-sulfur ratio modulation increases the number of electronic sites on the catalyst surface, which can effectively control the charge distribution on the catalyst surface and create more sites for PMS adsorption and activation [28-30]. Furthermore, the electron density difference indicates an obvious charge transfer between CoS_x and PMS molecules can be found, which indicates that the coordination adsorption and charge transfer between PMS and CoS_x contribute to the activation of PMS [28,31].

Besides, density of states analysis reveals covalent hybridization between Co and S orbitals (Fig. 3c) [32], with the d orbitals of CoS_x being the main component of the valence ban. By simulating the reaction energy barriers for the CoS_x-catalyzed PMS activation process, the results shown in Fig. 3d indicate that with the increase of cobalt-sulfur ratio, the catalyst surface is more likely to adsorb the PMS molecules to complete the electron transfer in the initial state [31,33]. And the energy required for the peroxy bond breaking of PMS catalyzed by CoS_2 is obviously larger than that of Co_3S_4 and Co_9S_8, so the CoS_2/PMS system has the worst reactivity. Overall, the increase of cobalt-sulfur ratio was more favorable to expose adsorption-catalytic sites and activate the PMS process.

In the following discussion, using the Co_9S_8/PMS system as a representative, the effect of other process parameters on the degradation of PCMX by CoS_x activated PMS will be investigated. The effects of PMS dosage and initial pH on the catalytic performance of Co_9S_8/PMS system were investigated (Fig. S3 in Supporting information). With the dosage of 1.00 mmol/L PMS, PCMX was degraded below the detection limit within 5 min. It indicates that there were enough active sites on the catalyst surface, and PMS was activated to generate enough ROS to degrade PCMX (Fig. S3a in Supporting information) [34]. When the initial pH value is in the range of 3.0–9.0, the pH changes little in the degradation process and has a certain stability (Fig. S3b in Supporting information).

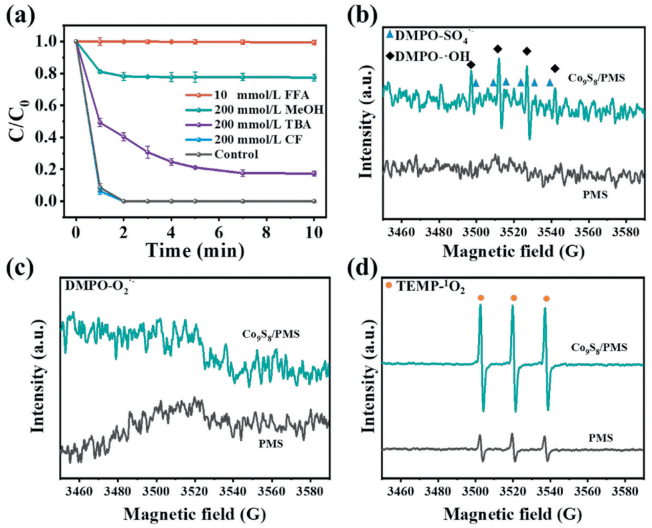

Fig. 4. (a) The effect of scavengers on PCMX degradation. EPR spectra of (b) DMPO-$SO_4^{\bullet-}$ and DMPO-$^{\bullet}$OH, (c) DMPO-$^{\bullet}O_2^-$, and (d) TEMP-$^1O_2$ in Co_9S_8/PMS system. Conditions: $[Co_9S_8]_0 = 0.20$ g/L, $[PCMX]_0 = 20$ mg/L, $[PMS]_0 = 1.00$ mmol/L, $pH_0 = 6.6$, $T = 20 \pm 1$ °C.

Quenching experiments and EPR techniques revealed the reactive species in the Co_9S_8/PMS system (Fig. 4). Fig. 4a showed that 200 mmol/L of MeOH and TBA inhibited approximate 87.5% and 17.4% of PCMX degradation, respectively, compared to the control. It indicates that a large amount of $SO_4^{\bullet-}$ was produced in the system, while a certain amount of $^{\bullet}$OH was present. CF on the Co_9S_8/PMS system was negligible, indicating that the content of

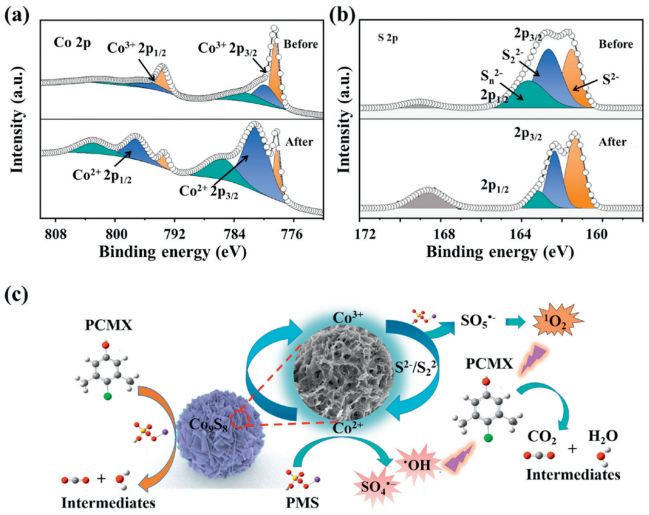

Fig. 5. XPS spectra of Co_9S_8 for (a) Co 2p and (b) S 2p before and after use. (c) Schematic illustration of mechanism for PCMX removal *via* Co_9S_8/PMS system.

$^{\bullet}O_2^-$ in the system is very small, or the generated $^{\bullet}O_2^-$ immediately transforms into other oxygen forms [35]. FFA can quench $SO_4^{\bullet-}$, $^{\bullet}OH$ and $^1O_2$ simultaneously [36,37]. The degradation of PCMX could be inhibited almost completely by adding 10 mmol/L FFA, providing evidence to the presence of a large amount of $^1O_2$ in the system. DMPO and TEMP spin traps were used for EPR analysis, and distinct signal peaks of 1:2:2:1 and 1:1:1:1:1:1 were detected in the Co_9S_8/PMS system, and the $^1O_2$ triplet peaks were significantly stronger than that in PMS (Figs. 4b–d). In agreement with the quenching experiments, the presence of $SO_4^{\bullet-}$, $^1O_2$ and $^{\bullet}OH$ in the Co_9S_8/PMS system was further verified.

The changes of element valance of Co_9S_8 before and after the degradation reaction were analyzed (after 5 cycles) (Figs. 5a and b). Table S5 (Supporting information) shows the changes in the valence content of Co and S before and after the degradation reaction. After the reaction, the content of Co^{2+} decreased by 23.0%, indicating that the main active site of PMS activation was $Co^{2+}_{surf.}$, which was oxidized to $Co^{3+}_{surf.}$ after the reaction (Eq. 2) [17]. At the same time, $Co^{3+}_{surf.}$ generated by oxidation would be reduced to $Co^{2+}_{surf.}$ by PMS (Eq. 3) [38]. $^{\bullet}OH$ in the system was generated by the reaction of $SO_4^{\bullet-}$ with H_2O or OH^- (Eqs. 4 and 5) [39]. The content of S^{2-} decreased by 12.4% after the reaction. S^{2-} has been reported to reduce $Co^{3+}_{surf.}$ to $Co^{2+}_{surf.}$ (Eq. 6), thereby enhancing the $Co^{2+}_{surf.}/Co^{3+}_{surf.}$ cycle efficiency and promoting the improvement of the catalytic efficiency [23]. A small fraction of $^1O_2$ in the system is produced by self-decomposition of PMS (Eq. 7) [21]. The majority of $^1O_2$ is formed by the reaction of accumulated $SO_5^{\bullet-}$ with H_2O (Eq. 8) [40]. Finally, ROS such as $SO_4^{\bullet-}$, $^{\bullet}OH$, and $^1O_2$ were produced in the system to oxidatively degrade PCMX to generate CO_2, H_2O, and degradation intermediates (Eq. 9).

$$\equiv Co(II)_{surf.} + HSO_5^- \rightarrow \equiv Co(III)_{surf.} + SO_4^{\bullet-} + OH^- \quad (2)$$

$$\equiv Co(III)_{surf.} + HSO_5^- \rightarrow \equiv Co(II)_{surf.} + SO_5^{\bullet-} + H^+ \quad (3)$$

$$SO_4^{\bullet-} + H_2O \rightarrow SO_4^{2-} + {}^{\bullet}OH + H^+ \quad (4)$$

$$SO_4^{\bullet-} + OH^- \rightarrow SO_4^{2-} + {}^{\bullet}OH \quad (5)$$

$$\equiv Co(III)_{surf.} + S^{2-} \rightarrow \equiv Co(II)_{surf.} + S_2^{2-}/SO_x \quad (6)$$

$$HSO_5^- + SO_5^{2-} \rightarrow HSO_4^- + SO_4^{2-} + {}^1O_2 \quad (7)$$

$$SO_5^{\bullet-} + H_2O \rightarrow SO_4^{2-} + {}^1O_2 + H^+ \quad (8)$$

$$SO_4^{\bullet-}/{}^{\bullet}OH/{}^1O_2 + PCMX \rightarrow CO_2 + H_2O + \text{intermediates} \quad (9)$$

The above discussion indicates that the main ROS in Co_9S_8/PMS system are $SO_4^{\bullet-}$, $^{\bullet}OH$, and $^1O_2$ (Fig. 5c). The main active site of the catalyst is $Co^{2+}_{surf.}$. The reduced sulfur species S^{2-} promotes the regeneration of $Co^{2+}_{surf.}$ on the catalyst surface, improving the catalytic efficiency.

To study the transformation and evolution of PCMX in the Co_9S_8/PMS system, the active site of contaminant PCMX susceptible to ROS attack was verified by DFT calculations (Fig. S4 in Supporting information) [40]. The HOMO and LUMO values of PCMX are -6.110 eV and -0.097 eV, respectively. the value of the energy gap ($\Delta E = E_{LUMO} - E_{HOMO}$) between HOMO and LUMO is 6.013 eV. The Fukui function (f^+, f^-, f^0) can be introduced to better investigate the oxidizing ability of each atom towards persulfate, catalysts and pollutants [41]. Based on the above calculations, it is considered that ROS such as $SO_4^{\bullet-}$, $^1O_2$, $^{\bullet}OH$ are more likely to undergo ring opening reaction in directly attacking the benzene ring at the position of C3-C4/C6-C7 versus C4-C5/C5-C6. Also, ROS can undergo side chain oxidation at C8 and C9. Combined with LCMS results (Fig. S5 in Supporting information), the degradation path of PCMX by Co_9S_8/PMS system was analyzed, as shown in Fig. S6 (Supporting information).

In order to reveal the effect of cobalt-sulfur ratio on the catalytic efficiency of the CoS_x/PMS system, the relationship between *n*(Co/S) and BET surface area was fitted. The result indicates that *n*(Co/S) was positively correlated with BET surface area (Fig. 6a). Meanwhile, BET surface area was in a good linear relationship with catalytic reaction rate constant and the correlation coefficient R^2 was 0.999 (Fig. 6b), indicating that the cobalt-sulfur ratio plays a key role in the PMS activation performance of cobalt sulfides, and the catalytic efficiency of cobalt sulfides increased with the cobalt-sulfur ratio. The difference in cobalt content on the surface of catalyst was analyzed by XPS to further explore the effect of BET surface area on the catalytic efficiency of catalysts. Fig. 6c shows the Co 2p spectra of CoS_2, Co_3S_4, and Co_9S_8 before reaction. The peaks at approximate 778.3, 781.0, 793.4, and 797.1 eV were assigned to be Co^{3+} $2p_{3/2}$, Co^{2+} $2p_{3/2}$, Co^{3+} $2p_{1/2}$, and Co^{2+} $2p_{1/2}$ [42], respectively.

We found that the content of Co^{2+} in the catalyst was increasing with the cobalt-sulfur ratio, while the content of Co^{3+} was decreasing. The proportions of Co^{2+} in CoS_2, Co_3S_4, and Co_9S_8 were 41.1%, 42.9%, and 57.5%, respectively. However, the proportions of Co^{3+} were 41.4%, 32%, and 12.8%, respectively. The relationship between the content of Co^{2+} and reaction rate constant *k* of each catalytic system was further determined at the same time. Fig. 6d reveals that the content of Co^{2+} is positively related to reaction rate constant *k* with a linear relationship. Therefore, the enhanced catalytic activity of cobalt sulfides can be attributed to the increase of Co^{2+} content on catalysts.

According to Fig. 6e, the cobalt-sulfur ratio can affect the physical properties of cobalt sulfides, such as morphology, BET surface area and surface Co^{2+} content, thus determining the catalytic activity of cobalt sulfides. With the increase of cobalt-sulfur ratio, the morphology of cobalt sulfides changes from nanoparticle to nanoflower, and the BET surface area of the catalyst increases gradually. The active site Co^{2+} on the catalyst surface thus can be more fully exposed, so as to improve the catalytic activity.

In this work, a series of CoS_x with different cobalt-sulfur ratio were successfully fabricated *via* one plot method for PCMX re-

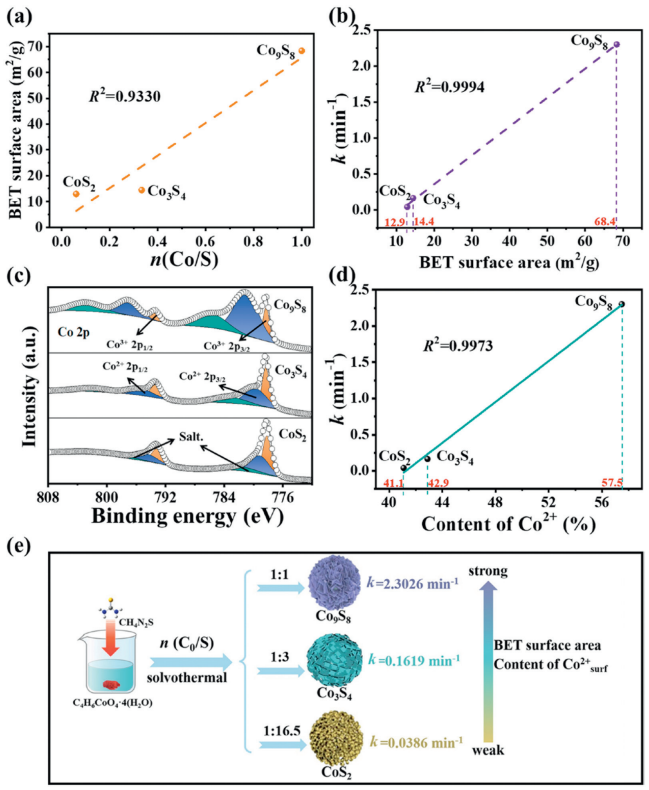

Fig. 6. (a) The relationship between *n*(Co/S) and BET surface area of CoS_x. (b) The relationship between BET surface area and reaction rate constant *k* of CoS_x. (c) Co 2p spectra of CoS_2, Co_3S_4, and Co_9S_8 before reaction. (d) The relationship between content of Co^{2+} and reaction rate constant *k* of CoS_x. (e) Schematic graph of the effect of cobalt-sulfur ratio on CoS_x/PMS system.

moval. The cobalt-sulfur ratio is a key factor in regulating the catalytic activity of CoS_x through the changes in charge properties and the exposure of active sites. With the reduction of the degree of vulcanization, the prepared cobalt sulfide has a larger BET surface area, and the active site ($Co^{2+}_{surf.}$) on its surface can be more fully exposed. The results shows that the first-order kinetic constant of PCMX degradation by Co_9S_8 was 2.30 min^{-1}, which is much higher than that of CoS_2 (0.039 min^{-1}) and Co_3S_4 (0.16 min^{-1}), and the value of *k* was highly linearly related to the specific surface area of CoS_x and the Co^{2+} content. DFT theoretical calculations also verified that the increase of cobalt-sulfur ratio can expose more active sites and reduce the energy barrier of catalytic oxidation reaction. This work provides both theoretical and technical support for the design of new cobalt-based catalysts for PMS activation.

Declaration of competing interest

The authors declare that they have no known competing financial interests or personal relationships that could have appeared to influence the work reported in this paper.

CRediT authorship contribution statement

Jiayi Guo: Writing – review & editing, Writing – original draft, Software, Data curation, Conceptualization. **Liangxiong Ling:** Writing – original draft, Conceptualization. **Qinwei Lu:** Writing – review & editing, Software. **Yi Zhou:** Writing – review & editing. **Xubiao Luo:** Writing – original draft. **Yanbo Zhou:** Writing – review & editing, Funding acquisition, Conceptualization.

Acknowledgments

This work was supported by the National Natural Science Foundation of China (No. 52370168) and the Program of Shanghai Outstanding Technology Leaders (No. 20XD1433900).

Supplementary materials

Supplementary material associated with this article can be found, in the online version, at doi:10.1016/j.cclet.2024.110380.

Reference

[1] K. Lv, L. Ling, Q. Lu, et al., Sep. Purif. Technol. 344 (2024) 127207.
[2] J. Lu, Y. Zhou, L. Ling, et al., Chem. Eng. J. 446 (2022) 137067.
[3] J. Tan, H. Kuang, C. Wang, et al., Sci. Total Environ. 786 (2021) 147524.
[4] M. Ijaz, K. Whitehead, V. Srinivasan, et al., Am. J. Infect. Control. 48 (2020) 972–973.
[5] W. Li, H.G. Guo, C. Wang, et al., Chem. Eng. J. 390 (2020) 124610.
[6] Y. Zhang, T. Wang, Q. Lu, et al., Chem. Eng. J. 482 (2024) 149002.
[7] C. Au, K. Chan, W. Chan, et al., J. Hazard. Mater. 445 (2023) 130550.
[8] J. Lu, Q. Liu, Y. Zhang, et al., Chin. Chem. Lett. 35 (2024) 109406.
[9] L. Di, T. Wang, Q. Lu, et al., Sep. Purif. Technol. 339 (2024) 126740.
[10] J. Lu, Q. Lu, L. Di, et al., Chin. Chem. Lett. 34 (2023) 108357.
[11] Y. Li, H. Dong, L. Li, et al., Water Res. 192 (2021) 116850.
[12] P. Wang, H. Zhang, Z. Wu, et al., Chin. Chem. Lett. 34 (2023) 108722.
[13] Y. Zhang, J. Liu, A. Moores, et al., Environ. Sci. Technol. 54 (2020) 4631–4640.
[14] G. Anipsitakis, D. Dionysiou, Environ. Sci. Technol. 38 (2004) 3705–3712.
[15] J. Xu, D. Wang, D. Hu, et al., Front. Env. Sci. Eng. 18 (2023) 37.
[16] Y. Zhou, L. Zhou, Y. Zhou, et al., Appl. Catal. B: Environ. 279 (2020) 119365.
[17] Y. Han, Y. Yang, W. Liu, et al., Front. Env. Sci. Eng. 18 (2024) 9.
[18] J. Xu, D. Wang, D. Hu, et al., Front. Env. Sci. Eng. 18 (2024) 37.
[19] Q. Yan, J. Zhang, M. Xing, Cell Rep. Phys. Sci. 1 (2020) 100149.
[20] L. Song, S. Deng, C. Bian, et al., Front. Env. Sci. Eng. 17 (2023) 96.
[21] J. Lu, Y. Zhou, Y.B. Zhou, Chem. Eng. J. 422 (2021) 130126.
[22] W. Li, S. Li, Y. Tang, et al., J. Hazard. Mater. 389 (2020) 121856.
[23] F. Wang, H. Fu, F. Wang, et al., J. Hazard. Mater. 423 (2022) 126998.
[24] P. Zhang, P. Zhou, J. Peng, et al., Water Res. 219 (2022) 118626.
[25] G. Pan, J. Wei, M. Xu, et al., J. Hazard. Mater. 445 (2023) 130479.
[26] Q. Wu, Y. Zhang, H. Liu, et al., Water Res. 224 (2022) 119022.
[27] R. Zheng, Q. Lin, L. Meng, et al., Sep. Purif. Technol. 298 (2022) 121619.
[28] J. Yang, D. Zeng, J. Li, et al., Chem. Eng. J. 404 (2021) 126376.
[29] L. Wang, H. Dong, Z. Guo, et al., J. Phys. Chem. C 120 (2016) 17427–17434.
[30] M. Feng, J.C. Baum, N. Nesnas, et al., Environ. Sci. Technol. 53 (2019) 2695–2704.
[31] X. Li, X. Huang, S. Xi, et al., J. Am. Chem. Soc. 140 (2018) 12469–12475.
[32] S. Pang, C. Zhou, Y. Sun, et al., J. Clean Prod. 414 (2023) 137569.
[33] Y. Zou, J. Hu, B. Li, et al., Appl. Catal. B: Environ. 312 (2022) 121408.
[34] D. Gao, Y. Lu, Y. Chen, et al., Appl. Catal. B: Environ. 309 (2022) 121234.
[35] Q. Yi, J. Ji, B. Shen, et al., Environ. Sci. Technol. 53 (2019) 9725–9733.
[36] Y. Zhou, J. Jiang, Y. Gao, et al., Environ. Sci. Technol. 49 (2015) 12941–12950.
[37] X. Cheng, H.G. Guo, Y.L. Zhang, et al., Water Res. 113 (2017) 80–88.
[38] X. Dong, X. Duan, Z. Sun, et al., Appl. Catal. B: Environ. 261 (2020) 118214.
[39] Q. Lu, L. Di, Y. Zhou, et al., Sep. Purif. Technol. 353 (2025) 128099.
[40] Y. Gu, T. Gao, F. Zhang, et al., Chin. Chem. Lett. 33 (2022) 3829–3834.
[41] R. Parr, W. Yang, J. Am. Chem. Soc. 106 (1984) 4049–4050.
[42] R. Guo, Y. Chen, Y. Yang, et al., Chin. Chem. Lett. 34 (2023) 107837.